Catalysis Science & Technology

ROYAL SOCIETY OF CHEMISTRY

PAPER

View Article Online
View Journal | View Issue

Check for updates

Cite this: *Catal. Sci. Technol.*, 2025, 15, 3113

Improved stereocontrol in reductive aminases through steric modification of residues around substrate and cofactor binding pockets†

Jake Gooderham,[a] Beatrice-Maria Zabava,[a] David D. Aleku,[a] Julie Vignot,[a] Zuoye Xie,[a] Ruth T. Bradshaw Allen,[a] Mario Prejanò *[b] and Godwin A. Aleku *[a]

Asymmetric reductive amination catalysed by reductive aminases (RedAms) provides a green and direct route to 2° and 3° chiral amines. Identifying residues or motifs in these enzymes that facilitate stereocontrol is essential for designing highly desirable enantiodivergent RedAm systems. In this work, we have identified key residues within both the cofactor and substrate binding pockets in a fungal reductive aminase (*Ma*RedAm) and a bacterial imine reductase (*Ao*IRED) that enable stereocontrol through steric modification. In *Ma*RedAm, removing steric bulk at the cofactor binding pocket *via* W33A or R35A mutation improved (*R*)-selectivity towards the synthesis of (*R*)-rasagiline, achieving up to 95% enantiomeric excess (e.e.). Conversely, the W211A mutation at the substrate binding pocket of *Ma*RedAm inverted the stereoselectivity, yielding (*S*)-rasagiline (42% e.e.). Likewise, varying steric bulk at position N241 in *Ao*IRED allowed for enantiodivergency. Notably, modifying the N241 position significantly improved *Ao*IRED's solution stability and storability. The wild-type enzyme typically precipitates out of solution within 8 h after purification, even when stored at 4 °C, whereas its N241H and N241Y variants remain in solution for up to >1 week. Molecular dynamics (MD) simulations provided detailed insights into the effect of steric modification on stereoselectivity at the cofactor and substrate binding pockets. *Ma*RedAm W33A and W35A mutations induced reorganisation and downsizing of the active site, enhancing (*R*)-selectivity. In contrast, the W211A mutation enlarged the substrate binding pocket, increasing flexibility for substrate rotation. These findings contribute to the ongoing effort to establish the functional roles of key residues to allow efficient rational engineering of stereoselectivity in IREDs/RedAms.

Received 13th March 2025,
Accepted 10th April 2025

DOI: 10.1039/d5cy00308c

rsc.li/catalysis

Introduction

Reductive amination of prochiral carbonyl compounds is a frequently employed transformation to construct chiral amine-based active pharmaceutical ingredients (APIs).[1,2] Enzymatic reductive amination reactions such as those catalysed by imine reductases (IREDs) and reductive aminases (RedAms)[3–7] are particularly attractive as they offer a highly enantioselective approach.[8–11] IREDs/RedAms' amination route provides direct access to enantiopure 2° and 3° chiral amines without the need to use toxic alkylating reagents or stoichiometric amounts of reducing agents. Given that chiral amines are among the most prevalent scaffolds in APIs, developing enantiodivergent RedAm methodologies will have enormous synthetic relevance.[12] However, IREDs/RedAms, similar to other redox enzymes, may on occasion catalyse the amination of prochiral ketones to yield the 'wrong' enantiomer of the target product or produce the desired enantio-enriched product in suboptimal optical purity. Achieving perfect enantioselectivity for a synthetic target remains challenging, often requiring extensive directed evolution campaigns,[13] which are impractical within the time constraints of drug development projects.[14]

Recent studies have sought to pinpoint the origin of stereoselectivity in IRED-catalysed reduction of cyclic imines based on the residue occupying the standard catalytic 187 position (*Sk*IRED numbering, Fig. 1).[15–17] From a wealth of empirical evidence, the so-called D-type IREDs which contain Asp at the 187 equivalent position are predominantly (*R*)-selective, and reduce simple cyclic imines such as 1-methyl-3,4-tetrahydroisoquinoline **1**, 2-methylpyrroline, and 2-methylpiperideine to the corresponding (*R*)-amines whereas

[a] *Institute of Pharmaceutical Science, Franklin-Wilkins Building, King's College London, 150 Stamford Street, London SE1 9NH, UK.*
E-mail: godwin.aleku@kcl.ac.uk
[b] *Department of Chemistry and Chemical Technologies, University of Calabria, Via Pietro Bucci 14/C, 87036 Arcavacata di Rende, CS, Italy.*
E-mail: mario.prejano@unical.it

† Electronic supplementary information (ESI) available: The supporting information, which can be found online, contains extended data, detailed experimental procedures, Chiral HPLC chromatograms for product analysis, sequence data, and MD simulations setup strategy. See DOI: https://doi.org/10.1039/d5cy00308c

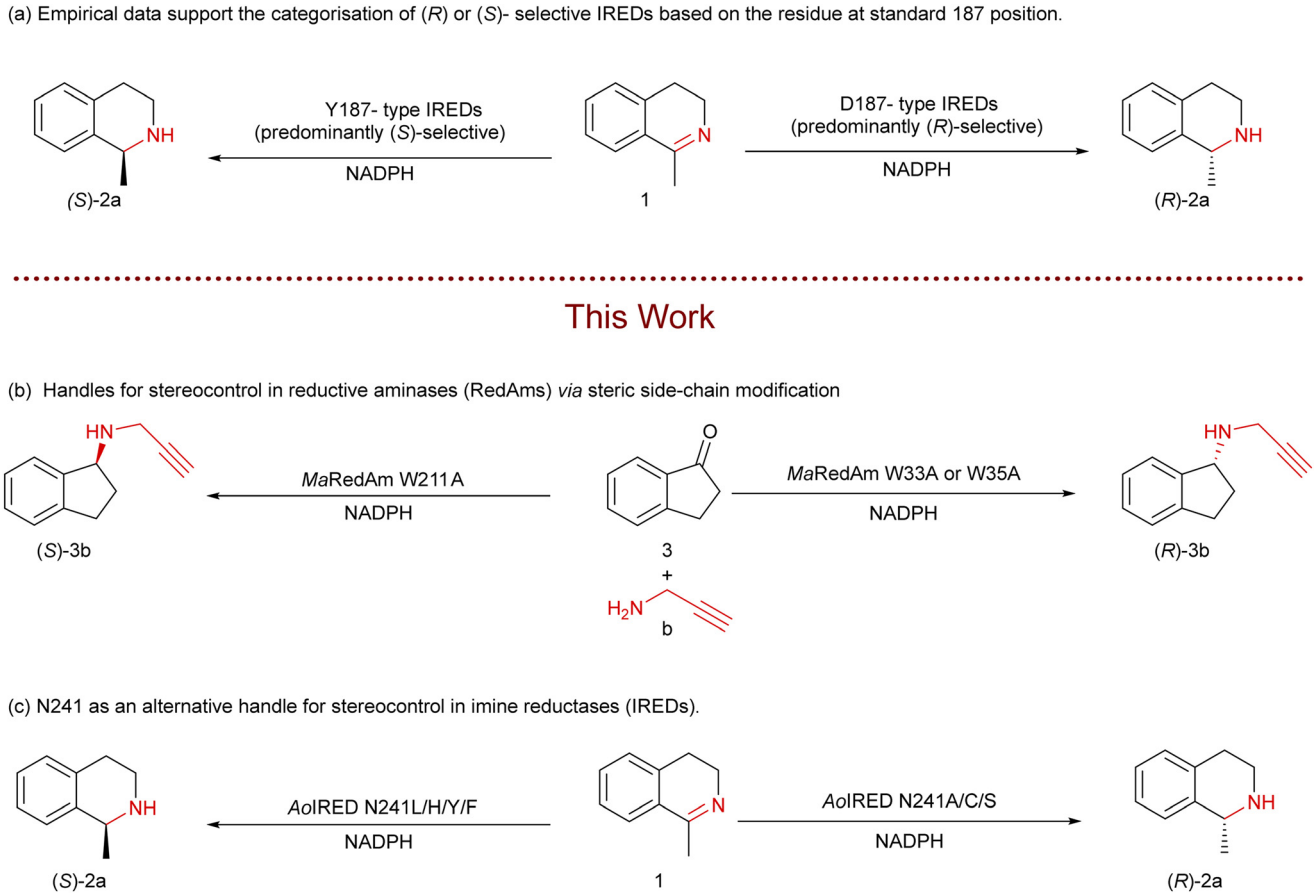

Fig. 1 Stereoselectivity patterns of imine reductases (IREDs) towards the reduction of prochiral cyclic imines and an overview of work performed in this study.

the so-called Y-type IREDs feature Tyr at the 187 position, are predominantly (*S*)-selective toward these substrates.[18–23] However, some IREDs do not follow these selectivity patterns or contain residues other than Asp or Tyr at the standard Y187 position.[15,17,24] In addition, other regulatory factors, such as electrostatic interactions between the anionic side chains of active site residues and the iminium cation, have been proposed to be critical to the stereochemical outcome of IRED-catalysed imine reduction.[17]

Despite the significant interest in engineering stereoselectivity in RedAms,[4,13,25–28] the regulatory factors governing stereoselectivity in RedAm-catalysed reductive amination remain poorly understood. Unlike for IRED-catalysed reduction of cyclic imines where available empirical data can guide prediction of the stereoselectivity of an IRED of interest, there is no clear pattern for the categorisation of (*S*)-type or (*R*)-type enzymes in IRED/RedAm-catalysed reductive amination of ketones based on the residue occupying the catalytically important position 187. IREDs acting in the RedAm mode must bind NADPH, ketone and amine to form the corresponding iminium cation,[4,29] and the size and nature of both the amine and ketone coupling partners can contribute to the stereochemical outcome.[4,29–31]

Steric modification of the side chains of key residues in many NAD(P)H-dependent redox enzymes, including IREDs, can directly or indirectly alter substrate and cofactor binding modes,[24] with its attendant effects on enzymatic activity. While such modifications are less frequently reported or investigated for IREDs/RedAms,[4,26] alteration of the substrate and cofactor binding modes in this manner can influence whether hydride delivery from NAD(P)H to the iminium ion occurs on the *Si*- or *Re*-face, which in turn can affect the stereochemical outcome. In this study, using a fungal reductive aminase (*Ma*RedAm)[31] and a bacterial imine reductase (*Ao*RED),[32] we systematically screened and identified multiple residues that enable stereocontrol in these enzymes through steric modification of their side chains.

Results and discussion

Handles in a reductive aminase for stereocontrol *via* modifying the side chain's steric bulk

To quickly assess the mutational effects of bulky conserved residues on RedAm's stereoselectivity, we employed alanine scanning site-directed mutagenesis, targeting conserved bulky residues (W, Y, F, and R) with a conservation score of >90%, regardless of whether these residues interact with the

substrates or the cofactor. Six such positions were identified through sequence alignment of >1200 *Ma*RedAm homologues (ESI,† Table S1). Alanine variants were successfully constructed, expressed in *E. coli* and the freshly prepared cell-free lysate (CFE) was used as the aminase catalyst solution to perform two amination transformations: 1-indanone **3** with propargylamine **b** and 4-phenyl-2-butanone **4** with **b**. Stereoselectivity of the product was assessed *via* chiral HPLC (Table 1).

Mutations W33A, R35A, Y139A, and Y181A in *Ma*RedAm (Scheme 1) led to observable changes in the stereoselectivity. The neighbouring variants W33A and R35A exhibited improvements in e.e. values, yielding, for example, (*R*)-rasagiline **3b** with up to 95% e.e., compared to 74% e.e. achieved by the wild-type enzyme (Table 1). In contrast, the Y139A mutation led to a marked decrease in e.e. (64% e.e., (*R*)-**4b**). Similar trends were observed with these mutants for the synthesis of **4b**, where W33A, R35A, Y118A, and Y181A all achieved significant improvement in e.e. of up >97% compared to 63% e.e. achieved by the wild-type enzyme. Again, Y139A mutation led to a significant decrease in e.e. value (25%). Replacing the bulky protic residues with alanine, such as in Y118A, Y139A, and Y181A, resulted in reduced activity and lower conversion values. Notably, the *Ma*RedAm mutation, W211A, confers a profound switch in stereoselectivity, resulting in the formation of the opposite enantiomer for both transformations (**3b**, W211A yielding 42% e.e. (*S*) *versus* 74% e.e. (*R*) for wild-type; **4b**, W211A gave 52% e.e. (*S*) *versus* 63% e.e. (*R*) for wild-type). Biotransformation reactions with purified enzyme preparation for selected variants (wild-type, W35A, and W211A) across three transformations confirmed this pattern of changes in stereoselectivity (ESI,† Table S2). In addition to the emerging evidence of the role of W211 in stereoselectivity as demonstrated in *Ma*RedAm, *Asp*RedAm[4,33] and other RedAms,[26] we identified two residues, W33 and W35, which are excellent handles for improving the stereoselectivity of *Ma*RedAm. To our knowledge, the role of W33 and W35 in stereocontrol in this enzyme family has not been previously reported, and neither has any residue in this structural loop been linked to stereocontrol in RedAms. Our work, therefore, highlights these residues as key handles for improving stereoselectivity in *Ma*RedAm and by extension, these residues may serve as handles for modifying stereoselectivity in other RedAms.

Molecular dynamics simulations reveal structural reorganisations of the active site

To investigate the rationale behind the observed changes in stereoselectivity, we performed molecular dynamics (MD) simulations on the AlphaFold model of *Ma*RedAm-WT (ESI,† Fig. S1) and its variants, W33A, R35A, and W211A. Using *Ma*RedAm-WT as the reference, the trajectories and structural changes resulting from these mutations were followed and analysed to detect any structural contributions in the binding step of the catalytic mechanism. In each simulation, NADP(H) and the substrates (indanone **3** + propargylamine **b**, for the formation of rasagiline **3b**) were explicitly included in the models.

Analysis of the MD trajectories of W33A and R35A mutations revealed a slight shift of NADP(H) towards W211,

Table 1 Investigating the effect of changing the steric bulk of conserved amino acids' side chains on the stereoselectivity of RedAms

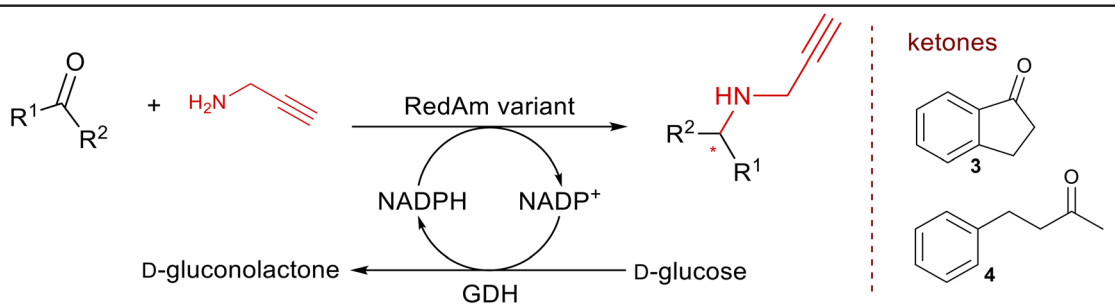

*Ma*RedAm and variants	Conv. (%)	e.e.% (abs. conf.)	Conv. (%)	e.e.% (abs. conf.)
*Ma*RedAm WT	31	74 (*R*)	>99	63 (*R*)[a]
W33A	43	95 (*R*)	>99	97 (*R*)[a]
R35A	33	92 (*R*)	>99	91 (*R*)[a]
Y118A	25	79 (*R*)	61	92 (*R*)[a]
Y139A	31	64 (*R*)	>99	25 (*R*)[a]
Y181A	<1	n.d.	7	>99 (*R*)[a]
W211A	30	42 (*S*)	95	36 (*S*)[a]

[a] Absolute configuration was assigned based on a comparison with the elution patterns of the *N*-methyl analogue. n.d. = not determined.

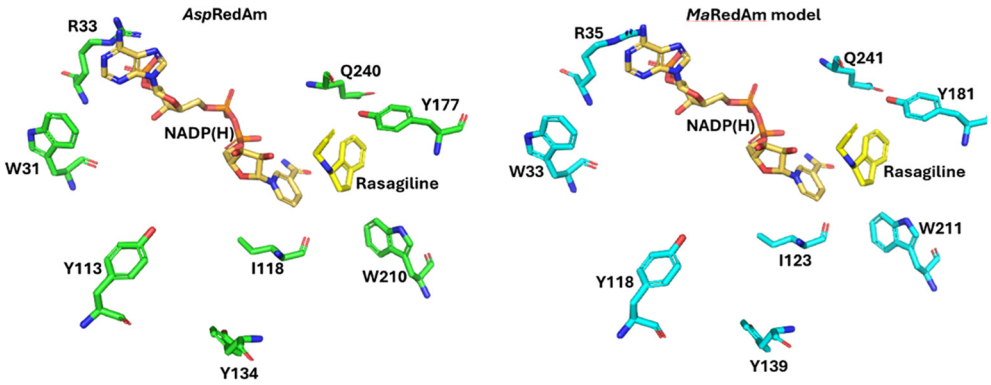

Scheme 1 *Asp*RedAm structure in complex with NADP(H) and the amine product rasagiline (PDB: 5G6S) and an AlphaFold-generated structural model of *Ma*RedAm, showing equivalent positions that affect enantioselectivity

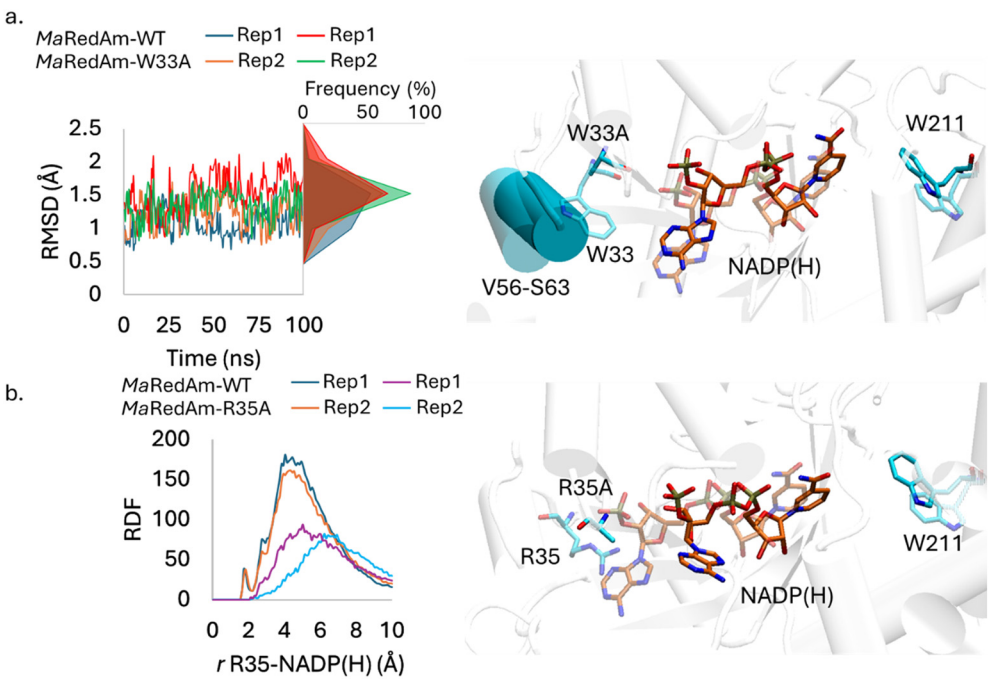

Fig. 2 RMSD of V56-S63 α-helix obtained from molecular dynamics (MD) simulations of *Ma*RedAm-WT and *Ma*RedAm-W33A systems (a). RDFs of R35-NADP(H) pair calculated from MD simulations of *Ma*RedAm-WT and *Ma*RedAm-R35A systems (b). For clarity, hydrogens were omitted, and only relevant species were reported. In the figures, atoms in transparent-background representation are for the wild-type enzyme.

resulting in a downsizing of the substrate's binding pocket (Fig. 2). The space created by the loss of the bulky indole group of Trp is now occupied by the α-helix formed by amino acid residues V56-S63 in the W33A mutant. This movement, evidenced by the analysis of root mean square deviation (see $1.0 < \text{RMSD (Å)} < 2.0$ *vs.* $0.5 < \text{RMSD (Å)} < 1.5$ value distributions in Fig. 2a), indicates a shift of NADP(H) towards W211 (Fig. 2a and ESI,† S2 and S4). A similar effect was observed with the R35A mutant mainly due to the loss of the stabilising ionic interaction between the guanidinium group of R35 (found in WT) and the phosphate moiety of the cofactor, as highlighted by the radial distribution function (RDF) calculated for the R35-NADP(H)/R35A-NADP(H) pairs (see absence of peak at *ca.* 2 Å for *Ma*RedAm-R35A, Fig. 2b). The cofactor shifts with respect to W211 by ~1.0 Å, moving away from the R35A position, thus affecting the volume of the substrate binding site (see NADP(H)-W211 distance variations in Fig. S4†).

While W33A and W35A mutations led to the reduction in the volume of the substrate binding pocket, we observed an opposite behaviour in *Ma*RedAm-W211A simulations, where the substrate's binding site was enlarged. The pocket generated by the W211A mutation was filled by water molecules, as shown by RDF calculated for W211-O_w/W211A-O_w pairs (Fig. 3a). In the case of the mutation-containing system, two peaks appeared at approximately 3.5 Å and 7 Å, corresponding to the first and second hydration shells surrounding the amino acid residue. The influx of water

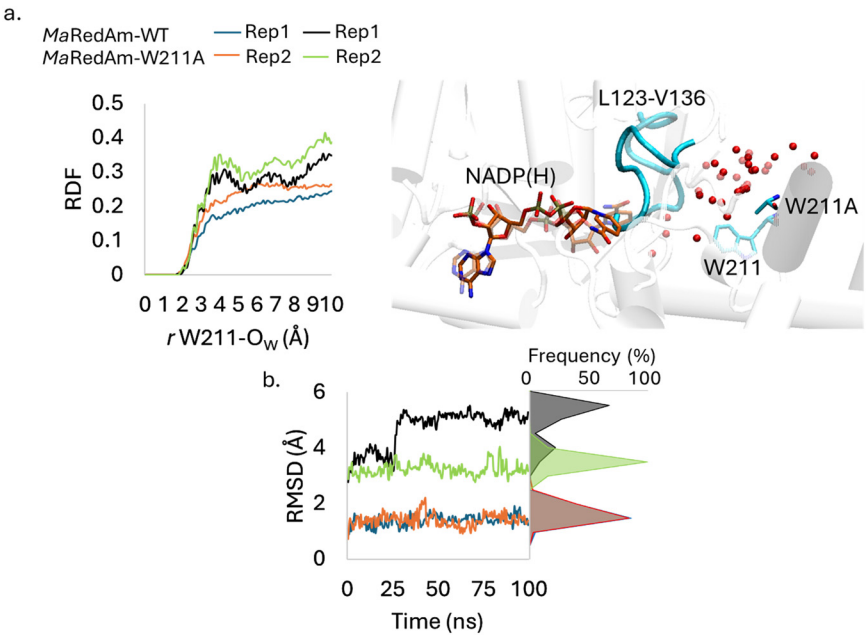

Fig. 3 RDFs of the W211-O_W pair calculated from molecular dynamics (MD) simulations (a) and RMSD of the L123-V136 loop (b) obtained from *Ma*RedAm-WT and *Ma*RedAm-W211A systems. For clarity, hydrogens were omitted, and only relevant species were reported. Atoms in the transparent background are those of the wild-type enzymes, while water molecules are depicted as red spheres.

molecules in the site is also linked to a reorganisation of the surrounding protein domain, such as the L123-V136 loop, which, shifting from the equilibrium conformation in *Ma*RedAm-WT, contributes to the further opening and enlargement of the active site pocket (see RMSD values in Fig. 3b). Regarding the NADP(H)-W211 distance, all these effects cumulated in an increase of up to 5 Å with respect to *Ma*RedAm-WT (see Fig. S5†).

These atomistic insights suggest that steric modulation of these bulky residues resulted in structural reorganisations of the cofactor and substrate binding pockets and their interactions, which in turn affected the stereoselectivity of *Ma*RedAm. On the one hand, removing steric bulk around the cofactor binding pocket *via* mutation caused a shift of NADP(H) and the reorganisation of surrounding residues, leading to a downsize of the active site. This reconfiguration may limit the flexibility of the iminium intermediate within the reduced active site volume, ultimately enhancing the pro-(*R*) enantioselectivity of the wild-type, as observed with W33A and W35A mutations. On the other hand, removing steric bulk by mutations in the substrate's binding site creates new pockets due to the space created by the mutation itself or by shifts of the surrounding protein domains. Thus, the iminium ion may rotate more freely, positioning it for *Si*-face hydride delivery, as demonstrated by the switch in the stereoselectivity observed with W211A.

N241 in a bacterial imine reductase (*Ao*IRED) enables stereocontrol *via* steric modification

Encouraged by these findings, we aimed to determine if steric modulation is equally significant in the enantioselective reduction of cyclic imines. In selecting a model IRED for this investigation, we considered the underexplored IRED block. Asp and Tyr are highly conserved at the standard 187 position in IREDs, resulting in most characterised IREDs broadly falling into the D-type and Y-type categories. However, a smaller proportion of IREDs contain alternative residues, including those featuring Asn at the standard 187 position, herein referred to as the N-type IREDs. As the stereoselectivity categorisation does not extend to the N-type IREDs, we first investigated the selectivity pattern of a small panel of N-type IREDs: *Ao*IRED, *Am*IRED, *Ar*IRED and *Se*IRED, retrieved through genome mining (Table 2). A multiple sequence alignment of over 500 homologues of these selected enzymes showed that Asn is conserved in >95% of the sequences, underscoring the N-type enzymes as an important IRED subgroup. Each of the four cloned enzymes was heterologously expressed in *E. coli* BL21 (DE3). Biotransformation with fresh lysate preparation of each enzyme converted imine **1** to the corresponding (*S*)-**2a**, affording >90% conversion and 40–87% e.e. (Table 2). This observation suggests that N-type IRED block are predominantly (*S*)-selective towards the enantioselective reduction of imine **1** and related structures, and a further study with a large panel of N-type IREDs is needed to establish the stereoselectivity pattern of the IRED block.

Position 187 (N171 in *Ao*IRED) has been shown to play an important role in stereocontrol in multiple IREDs, including the N-type IREDs. However, mutations at this position frequently lead to concurrent activity loss, as demonstrated with several IREDs.[4,17,20,29,32,34] Previous studies have also shown that the Y179A mutation in *Ao*IRED markedly altered

Table 2 Stereoselectivity of *Ao*IRED N241X variants for the reduction of prochiral imine **1**

Investigating the stereoselectivity of IREDs containing Asn at the 187 position

```
                                                                    187
          ....|....| ....|....| ....|....| ....|....| ....|....| ....|....| ....|....| ....|....|
               150        160        170        180        190        200        210
SkIRED_   AAIGTADAVV LLSGPRSAFD PHASALGGLG AGTTYLGADH GLASLYDAAG LVMMWSILNG FLQGAALLGT
AoIRED_   AMVGHPGSVF LYSGSAEVFE EYKETLAGLG -DPVHLGTEA GLAVLYNTAL LSMMYSSMNG FLHAAALVGS
AmIRED_   PLVGHTGSLF LYSGSTEIFE THKETLADLG -DPAHLGTDP GLAVLYNTAL LSMMYSSLNG FLHAAALVGS
ArIRED_   AMVGRPGSVF LYSGAEDVFD AHKATLAVLG -EATYLGADP GLAVLYNTAL LSLMYSSMNG FLHAAALVGS
SeIRED_   EVIGTPSSVV FYSGAREPFD AHRSTLDALG GVPRYLGDDA GLAVLHNTAL LGLMWATVNG FLHAAALVES
SsIRED_   PLVGRPDAVF LYSGDRAVLD EHRATLASLG -DPRFLGADP TLAVLYNTAL LHMMYATLNG YLQATALVGS
SlIRED_   PLVGHPDSVF LYSGSRDVFD KHRAALAALG -DPRYLGSDP GLAVLYNTAL LDMMYATLNG WLHATALVGS
```

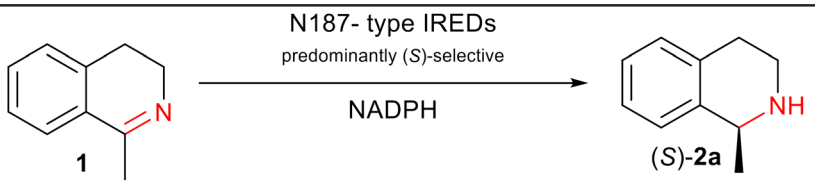

Enzymes	GenBank no.	Conversion [%]	e.e. [%] (*R* or *S*)
*Ao*IRED	5A9S_B	>99%	85 (*S*)
*Am*IRED	WP_125690082.1	90	40 (*S*)
*Ar*IRED	WP_257488618.1	>99	69 (*S*)
*Se*IRED	WP_211898848.1	>99	77 (*S*)

the stereoselectivity towards **2**,[24,32] however, mutations at this position are likewise associated with a significant reduction in activity across various IREDs, including *Ao*IRED.[4,29,32] Hence, we sought to identify an alternative residue that can serve as a handle for stereocontrol with minimal impact on IRED activity. We previously demonstrated that *Ao*IRED N241A mutant displays enhanced substrate tolerance towards bulky substrates such as dibenzazepines,[35] implicating N241 in substrate recognition/specificity. The N241A mutant was also shown to exhibit opposite selectivity compared to the wild type,[32] and this position has recently been shown to play a similarly critical role in engineering stereoselectivity inversion in D- and Y-types IREDs.[36]

Encouraged by these observations, we examined the effect of sterically varied residue substitutions at N241 on the stereoselectivity of *Ao*IRED (Scheme 2). Eight defined point mutants at N241 comprising characteristically distinct amino acid residues were constructed, including N241A, N241S, N241C, N241Y, N241F, N241H, N241L, and N241W, and each variant was expressed in *E. coli* to generate recombinant whole-cell biocatalysts. Given the stereoselectivity changes that can occur with purified *Ao*IRED upon storage,[32] bioreduction of **2** was performed using resting *E. coli* whole cells expressing an *Ao*IRED mutant. Analysis of these biotransformation reactions *via* chiral HPLC revealed that variants containing amino acid residues with small side chains, including N241A, N241S, and N241C, produced the (*R*)-**2a** product, albeit with low to moderate e.e. values ranging from 4% to 40% (Table 3). These results represent an inversion in stereopreference, as *Ao*IRED WT yielded (*S*)-**2a**, 85% e.e. In contrast, variants bearing amino acids larger than Asn (N241Y, N241F, N241L, and N241H) retained the wild-type stereoselectivity, yielding (*S*)-2a, but with significantly improved enantiomeric excess (e.e.) values, ranging from 92% to >99% e.e. (Table 3). The N241W substitution was associated with activity loss, likely due to unproductive binding of the substrate caused by steric hindrance from the bulky Trp (Table 3).

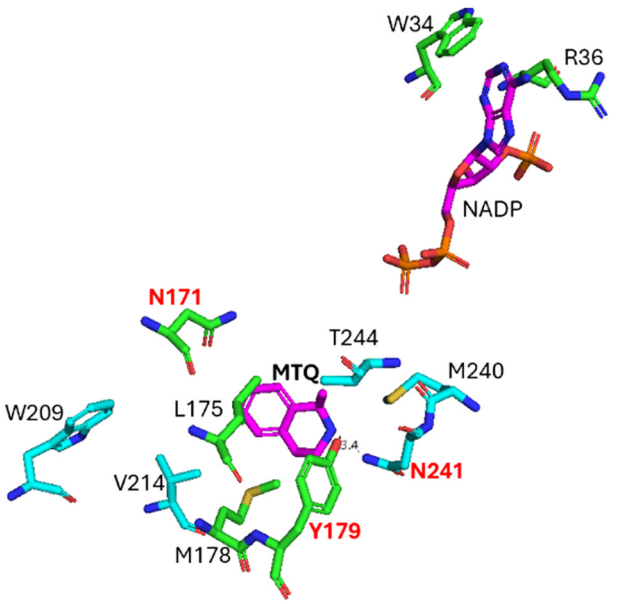

Scheme 2 *Ao*IRED in complex with amine **2a**, and NADP(H) showing the targeted N241 residue (PDB: 5FWN). While N171 and Y179 have been shown to affect the stereoselectivity of IREDs, mutations at these positions are associated with marked loss of activity. This study examines the role of N241 in stereocontrol without compromising activity.

Table 3 Stereochemical outcomes from bioreduction of imine **1** catalysed by *Ao*IRED N241X variants

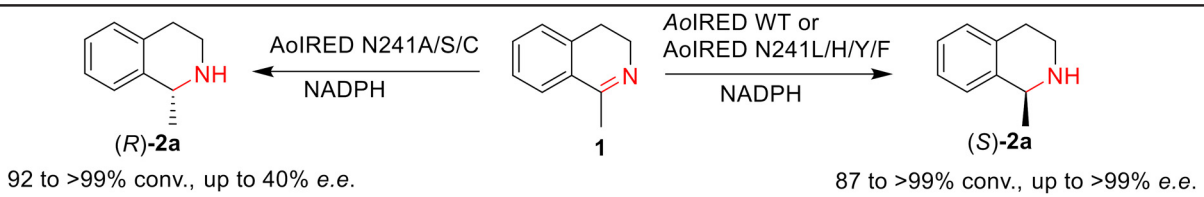

*Ao*IRED variants	Conv. [%]	e.e. [%] (*R* or *S*)
WT	98	85 (*S*)
N241L	>99	98 (*S*)
N241H	87	92 (*S*)
N241Y	>99	>99 (*S*)
N241F	98	97 (*S*)
N241W	<5%	n.d.
N241A	96	42 (*R*)
N241S	>99	13 (*R*)
N241C	92	4 (*R*)

The pattern of the stereoselectivity of *Ao*IRED N241X variants indicates a critical role of steric bulk modification in determining the stereoselectivity of this enzyme. Residues with bulky hydrophobic and aromatic side chains at N241 would stabilise and 'cage' the imine substrate, resulting in less flexibility such that hydride attack predominantly occurs at one face, in this case, the *Si*-face. As a consequence, the (*S*)-configured amine product was obtained with excellent e.e. values, ranging from 92 to >99%. In contrast, a less intimate interaction may allow flexibility for hydride delivery to both *Si*-face and *Re*-face when a smaller amino acid occupies this position, as in N241A, N241S, and N251C. This is evidenced by the inversion of stereoselectivity and the poor to moderate e.e. values (4–42%) with these substitutions.

Using imine **1** as the prototype substrate, we determined the Michaelis–Menten constants of *Ao*IRED WT, N241A, N241H, and N241S variants. The catalytic efficiency, k_{cat}/K_m (s^{-1} mM^{-1}) of these variants were 1.034, 1.934 (~1 fold improvement over parent (FIOP)), 2.054 (~1 FIOP), 4.730 s^{-1} mM^{-1} (~4 FIOP), respectively (ESI,† Table S3). These improvements were primarily driven by a decrease in the K_m, except for N241S, which showed improvements in both K_m and k_{cat} (ESI,† Table S3). The N241 position, therefore, enables the fine-tuning of stereoselectivity and simultaneously enhances the catalytic efficiency of this enzyme.

N241Y/H in *Ao*IRED exhibits significantly improved solution behaviour and storability

In our hands, *Ao*IRED wild-type was shown to aggregate and precipitate out of solution between 6–8 h after purification when stored (4 °C) at concentrations above 4 mg mL^{-1}. We purified N241X variants to homogeneity and investigated their solution behaviour (Table 4). Notably, we observed that N241X variants bearing polar residues/residues capable of engaging in hydrogen bonding interaction such as N241S, N241Y, and N241H, showed dramatically improved solution behaviour and storability.

While the N241F variant precipitated within 6 h of purification, the N241S, N241Y and N241H remained homogeneous for up to 18 h, 72 h, and >168 h (>7 days), respectively, indicating a substantial improvement in solution behaviour. Analysis of the pattern of substitution in relation to the Kyte–Doolittle hydropathy index[37] revealed that residues with negative hydropathy scores and capable of hydrogen bonding interactions, such as those in N241S, N241Y, and N241H, exhibited enhanced stability (Table 4). Protein aggregation can hinder the industrial exploitation of promising but aggregation-prone biocatalysts, such as *Ao*IRED. It is therefore remarkable and novel for this enzyme family that single-point mutants at the N241 position, particularly N241H, dramatically enhanced solution behaviour. This position can thus be explored to improve the storability and stability of purified *Ao*IRED and, by extension, other aggregation-prone IREDs/RedAms.

Conclusion

In summary, our findings demonstrate that steric modulation of residues at both the cofactor and substrate binding sites can induce stereocontrol in IREDs/RedAms, enabling the improvement as well as inversion of

Table 4 Investigation of solution behaviour of selected *Ao*IRED N241X variants, with N241S, N241Y and N241H showing significantly improved solution behaviour and storability. Enzymes were stored at 4 °C, and precipitation was monitored at intervals by visual examination

Variants	Residues	Hydropathy index (Kyte-Doolittle)	Time to precipitate
*Ao*IRED Wt	Asn	−3.5	<8 h
N241F	Phe	2.8	<6 h
N241C	Cys	2.5	<8 h
N241A	Ala	1.8	12 h
N241S	Ser	−0.8	24 h
N241Y	Tyr	−1.3	72 h
N241H	His	−3.2	>1 week

stereoselectivity through rational fine-tuning of the steric bulk of these residues. The residues identified in this study: W211 (in *Ma*RedAm) and Q241 (N241 in *Ao*IRED) at the substrate binding pocket and W33 and W35 at the cofactor binding site, can serve as key handles for fine-tuning stereoselectivity in these enzymes to achieve the desired stereochemical outcomes, especially through steric modulation. The comparative molecular dynamics outcomes obtained from the enzyme-substrate complex simulations have enabled the qualitative detection of structural details underlying the origin of *Ma*RedAm's enantioselectivity and explain the effect of steric modulation resulting from these mutations. Remarkably, exploring substitutions at the N241 position also significantly enhanced the solution behaviour and storability of *Ao*IRED, from less than 8 hours to over 1 week. This improvement not only enhances the practical application of *Ao*IRED but also suggests that strategic mutations can have a significant impact on enzyme stability. This work lays an important foundation towards making engineering stereoselectivity in IREDs/RedAms predictable, faster, and cost-effective. Future efforts will focus on mapping additional residues that may act as handles for stereocontrol and pinpointing the origin of enantioselectivity in RedAms through quantitative calculations of accurate energy profiles for the catalytic reaction, as well as analysis of related intermediates and transition states.

Data availability

The data supporting this article have been included as part of the ESI.†

Author contributions

Conceptualisation: G. A. A.; methodology: G. A. A. and M. P.; investigation and formal analysis: all authors; writing – initial draft: G. A. A., M. P.; supervision: G. A. A. All authors have read and approved the final version of the manuscript.

Conflicts of interest

There are no conflicts to declare.

Acknowledgements

This work received support from the Leverhulme Trust through a Leverhulme Early Career Fellowship to G. A. A. (ECF-2020-694), and further support was provided by a Royal Society Grant to G. A. A. (RGS\R1\231514). G. A. A. is also grateful to the Institute of Pharmaceutical Science at King's College London for its financial support of this project. M. P. is grateful to the Department of Chemistry and Chemical Technologies, Università della Calabria, for financial support and to ISCRA-Leonardo for supercomputing resources (project ID: HP10CEZM7C).

References

1 S. D. Roughley and A. M. Jordan, *J. Med. Chem.*, 2011, **54**, 3451–3479.
2 O. I. Afanasyev, E. Kuchuk, D. L. Usanov and D. Chusov, *Chem. Rev.*, 2019, **119**, 11857–11911.
3 G. A. Aleku, *ACS Catal.*, 2024, **14**, 14308–14329.
4 G. A. Aleku, S. P. France, H. Man, J. Mangas-Sanchez, S. L. Montgomery, M. Sharma, F. Leipold, S. Hussain, G. Grogan and N. J. Turner, *Nat. Chem.*, 2017, **9**, 961–969.
5 R. Kumar, M. J. Karmilowicz, D. Burke, M. P. Burns, L. A. Clark, C. G. Connor, E. Cordi, N. M. Do, K. M. Doyle, S. Hoagland, C. A. Lewis, D. Mangan, C. A. Martinez, E. L. McInturff, K. Meldrum, R. Pearson, J. Steflik, A. Rane and J. Weaver, *Nat. Catal.*, 2021, **4**, 775–782.
6 M. Schober, C. MacDermaid, A. A. Ollis, S. Chang, D. Khan, J. Hosford, J. Latham, L. A. F. Ihnken, M. J. B. Brown, D. Fuerst, M. J. Sanganee and G.-D. Roiban, *Nat. Catal.*, 2019, **2**, 909–915.
7 T. Liu, Z. Xu, J. Feng, S. Yu, M. Wang, P. Yao, Q. Wu and D. Zhu, *Org. Lett.*, 2023, **25**, 2438–2443.
8 L. Ducrot, M. Bennett, G. Grogan and C. Vergne-Vaxelaire, *Adv. Synth. Catal.*, 2021, **363**, 328–351.
9 A. K. Gilio, T. W. Thorpe, N. Turner and G. Grogan, *Chem. Sci.*, 2022, **13**, 4697–4713.
10 T. Knaus, W. Böhmer and F. G. Mutti, *Green Chem.*, 2017, **19**, 453–463.
11 B. Yuan, D. Yang, G. Qu, N. J. Turner and Z. Sun, *Chem. Soc. Rev.*, 2024, **53**, 227–262.
12 N. A. McGrath, M. Brichacek and J. T. Njardarson, *J. Chem. Educ.*, 2010, **87**, 1348–1349.
13 E. J. Ma, E. Siirola, C. Moore, A. Kummer, M. Stoeckli, M. Faller, C. Bouquet, F. Eggimann, M. Ligibel, D. Huynh, G. Cutler, L. Siegrist, R. A. Lewis, A.-C. Acker, E. Freund, E. Koch, M. Vogel, H. Schlingensiepen, E. J. Oakeley and R. Snajdrova, *ACS Catal.*, 2021, 12433–12445.
14 M. D. Truppo, *ACS Med. Chem. Lett.*, 2017, **8**, 476–480.
15 S. Fademrecht, P. N. Scheller, B. M. Nestl, B. Hauer and J. Pleiss, *Proteins: Struct., Funct., Bioinf.*, 2016, **84**, 600–610.
16 X.-X. Zhu, W.-Q. Zheng, Z.-W. Xia, X.-R. Chen, T. Jin, X.-W. Ding, F.-F. Chen, Q. Chen, J.-H. Xu, X.-D. Kong and G.-W. Zheng, *Nat. Commun.*, 2024, **15**, 10330.
17 K. Wu, J. Yan, Q. Liu, X. Wang, P. Wu, Y. Cao, X. Lu, Y. Xu, J. Huang and L. Shao, *Chem. Sci.*, 2024, **15**, 1431–1440.
18 S. Hussain, F. Leipold, H. Man, E. Wells, S. P. France, K. R. Mulholland, G. Grogan and N. J. Turner, *ChemCatChem*, 2015, **7**, 579–583.
19 F. Leipold, S. Hussain, D. Ghislieri and N. J. Turner, *ChemCatChem*, 2013, **5**, 3505–3508.
20 H. Man, E. Wells, S. Hussain, F. Leipold, S. Hart, J. P. Turkenburg, N. J. Turner and G. Grogan, *ChemBioChem*, 2015, **16**, 1052–1059.
21 H. Man, E. Wells, S. Hussain, F. Leipold, S. Hart, J. P. Turkenburg, N. J. Turner and G. Grogan, *ChemBioChem*, 2015, **16**, 1052–1059.

22 P. N. Scheller, S. Fademrecht, S. Hofelzer, J. Pleiss, F. Leipold, N. J. Turner, B. M. Nestl and B. Hauer, *ChemBioChem*, 2014, **15**, 2201–2204.
23 S. Velikogne, V. Resch, C. Dertnig, J. H. Schrittwieser and W. Kroutil, *ChemCatChem*, 2018, **10**, 3236–3246.
24 M. Prejanò, X. Sheng and F. Himo, *ChemistryOpen*, 2022, **11**, e202100250.
25 H. Zhou, P. Chuang, L. Xu and Q. Wu, *Org. Lett.*, 2023, **25**, 6688–6692.
26 A. R. Casamajo, Y. Yu, C. Schnepel, C. Morrill, R. Barker, C. W. Levy, J. Finnigan, V. Spelling, K. Westerlund, M. Petchey, R. J. Sheppard, R. J. Lewis, F. Falcioni, M. A. Hayes and N. J. Turner, *J. Am. Chem. Soc.*, 2023, **145**, 22041–22046.
27 P. Stockinger, N. Borlinghaus, M. Sharma, B. Aberle, G. Grogan, J. Pleiss and B. M. Nestl, *ChemCatChem*, 2021, **13**, 5210–5215.
28 J. Zhang, Y. Ma, F. Zhu, J. Bao, Q. Wu, S.-S. Gao and C. Cui, *Chem. Sci.*, 2023, **14**, 4265–4272.
29 M. Sharma, J. Mangas-Sanchez, S. P. France, G. A. Aleku, S. L. Montgomery, J. I. Ramsden, N. J. Turner and G. Grogan, *ACS Catal.*, 2018, **8**, 11534–11541.
30 G.-D. Roiban, M. Kern, Z. Liu, J. Hyslop, P. L. Tey, M. S. Levine, L. S. Jordan, K. K. Brown, T. Hadi, L. A. F. Ihnken and M. J. B. Brown, *ChemCatChem*, 2017, **9**, 4475–4479.
31 G. A. Aleku and F. Hollfelder, *Chem Catal.*, 2024, **4**, 101160.
32 G. A. Aleku, H. Man, S. P. France, F. Leipold, S. Hussain, L. Toca-Gonzalez, R. Marchington, S. Hart, J. P. Turkenburg, G. Grogan and N. J. Turner, *ACS Catal.*, 2016, **6**, 3880–3889.
33 G. A. Aleku, J. Mangas-Sanchez, J. Citoler, S. P. France, S. L. Montgomery, R. S. Heath, M. P. Thompson and N. J. Turner, *ChemCatChem*, 2018, **10**, 515–519.
34 M. Rodríguez-Mata, A. Frank, E. Wells, F. Leipold, N. J. Turner, S. Hart, J. P. Turkenburg and G. Grogan, *ChemBioChem*, 2013, **14**, 1372–1379.
35 S. P. France, G. A. Aleku, M. Sharma, J. Mangas-Sanchez, R. M. Howard, J. Steflik, R. Kumar, R. W. Adams, I. Slabu, R. Crook, G. Grogan, T. W. Wallace and N. J. Turner, *Angew. Chem., Int. Ed.*, 2017, **56**, 15589–15593.
36 Y. Li, Y. Yang, M. Zhang, X. Yue, R.-T. Guo, Z. Huang and F. Chen, *ACS Catal.*, 2025, **15**, 2192–2199.
37 J. Kyte and R. F. Doolittle, *J. Mol. Biol.*, 1982, **157**, 105–132.